Multiscale homogenization of pre-treatment rapid and slow filtration processes with experimental and computational validations

Alvin Wei Ze CHEW[1], *Adrian Wing-Keung LAW[1, 2]

1 School of Civil and Environmental Engineering, Nanyang Technological University, N1-01c-98, 50 Nanyang Avenue, Singapore 639798

2 Environmental Process Modelling Centre (EPMC), Nanyang Environment and Water Research Institute (NEWRI), 1 Cleantech Loop, CleanTech One, #06-08, Singapore 637141

Corresponding author's email: cwklaw@ntu.edu.sg

Abstract.

In this paper, we summarize on an approach which couples the multiscale method with the homogenization theory to model the pre-treatment depth filtration process in desalination facilities. By first coupling the fluid and solute problems, we systematically derive the homogenized equations for the effective filtration process while introducing appropriate boundary conditions to account for the deposition process occurring on the spheres' boundaries. Validation of the predicted results from the homogenized model is achieved by comparing with our own experimentally-derived values from a lab-scale depth filter. Importantly, we identify a need to include a computational approach to resolve for the non-linear concentration parameter within the defined periodic cell at higher orders of reaction. The computational values can then be introduced back into the respective homogenized equations for further predictions which are to be compared with the obtained experimental values. This proposed hybrid methodology is currently in progress.

Keywords: homogenization theory; multi-scale perturbation; porous media filtration; computational and analytical modelling

1. Introduction

For seawater reverse osmosis (SWRO) desalination, pre-treatment of the seawater source is typically carried out to remove turbidity and natural organic matter to mitigate excessive fouling of the RO modules downstream. The most common pre-treatment technology in medium- and large-scale desalination plants today is rapid granular filtration based on single or dual-media (Voutchkov, 2017). The optimised goal of the pre-treatment step is to maximise the productivity of filtered effluent into the downstream RO membranes facility before the maintenance of the granular filter.

Generally, filters' maintenance is resource-expensive and requires proper management to minimize logistical problems. For depth filters, maintenance is achieved via backwashing by mechanically pumping filtered or brine water reversely through the filter, which expands the granular media and flushes away the unwanted materials strained inside. Currently, the standard practice calls for backwashing at a fixed interval typically once every 24 to 48 hours (MWH, 2005; Voutchkov, 2017), without a full diagnosis of the degree of clogging occurring inside the operating filter a priori. Thus, backwashing is either carried out unnecessarily since the filter can still operate effectively for an extended period, or unexpectedly due to elevated turbidity levels in the intake source during stormy seasons which results in either exceedance in effluent turbidity or maximum allowable head loss within the filter before the scheduled maintenance.

Advanced computational methods have facilitated our understanding of the movement of emulated turbidity particles in an idealised pore-structure representation of the filter. In OpenFOAM (The OpenFOAM Foundation), which is an Open-Source Computational Fluid Dynamics (CFD) software, their Eulerian-Lagrangian (EL) approach uses the track-to-face algorithm to simulate the Lagrangian particle movement from one computational grid to the other. The algorithm requires that the size of the Lagrangian particle to be smaller than the smallest length of the computational grid. Hence, for very small Lagrangian particles of $O(10^{-7}\,m)$, the number of grids in each axial flow direction exceeds $O(10^3)$, resulting in billions of grids for a full three-dimensional (3D) problem which is computationally very expensive.

Theoretical analysis offers another alternative by coupling the homogenization up-scaling approach with the multi-scale perturbation technique to reduce the complexity of the macroscopic problem. This approach minimizes the empiricism involved in the model formulation with two key assumptions: (a) a near- or fully-periodic prescribed microstructure, and (b) sufficiently small dimensionless parameters to relate the macroscale and microscale variations. In the following, we describe several important contributions from the literature which adopt this approach to model the remediation process in porous media systems in general.

Mei et al. (1996) derived the homogenized Darcy's Law for saturated porous media by considering the flow past a periodic array of rigid media, followed by the numerical computation of the hydraulic conductivity inside the microscale cell. Mei (1992), Mei et al. (1996) and Mei and Vernescu (2012b) also rigorously derived the convection dispersion equation and solved for the dispersion of a passive solute in the seepage flow through a spatially periodic domain. Bouddour et al. (1996) derived the characteristic models for four varying flow phenomena within the microscale domain to analyse the formation damage in the macroscopic porous media due to erosion and deposition of solid particles. A similar approach was also adopted by Royer et al. (2002) to investigate the transport of contaminants in fractured porous media under varying local Peclet (Pe) numbers, based on the assumption that both convection and molecular diffusion were of equal importance within the microscale domain. Ray et al. (2012) analysed the

transport of colloids and investigated the variation to the microstructure during the attachment and detachment of colloidal particles in a two-dimensional (2D) saturated porous media structure by coupling the surface reaction rate and Nernst-Planck equations. Most recently, Dalwadi et al. (2015) first demonstrated the effectiveness of a decreasing porosity gradient to maximise a filter's trapping capability. They later consider the changes to the microscale media properties to quantify the filter blockage (Dalwadi et al., 2016). The theoretical novelty of these models is notable as they enable one to predict the filter's initial porosity value which attains homogeneous clogging. However, their theoretical analysis has not yet been extended to actual industrial conditions of pre-treatment depth filters.

In this study, we extend on the homogenization theory by Mei and Vernescu (2012a and 2012b) to model the macroscale filter's clogging condition as particles deposition onto the boundaries of the microscale spheres. Our engineering model aims to analytically predict the normalized pressure gradient behavior acting upon the filter by considering the known operating conditions. Subsequently, an experimental study was performed with a lab-scale depth filter setup to pre-treat seawater influents under varying conditions. We then compare the derived experimental results with the model predictions for validating the proposed engineering model.

In the following, we first describe the full flow and particle transport equations in Section 2 and the adopted homogenization procedures in Section 3. In Section 4, we present the details of our adopted experimental study. Section 5 compares the experimental and predicted values obtained from the engineering model. The computational methodology to resolve the non-linear multiscale analysis is then discussed in Section 6. Finally, we conclude with an overview of our completed works in Section 7.

2. Model Formulation

2.1. Model's general description

The macroscale granular filter is first modelled as an idealized network of non-overlapping three-dimensional rigid ideal spheres which either follows the simple cubic (SC) arrangement (see Figure 1). The figure is illustrated in its two-dimensional cross-sectional form due to the inherent symmetry of the adopted spheres. However, the analysis remains strictly three-dimensional.
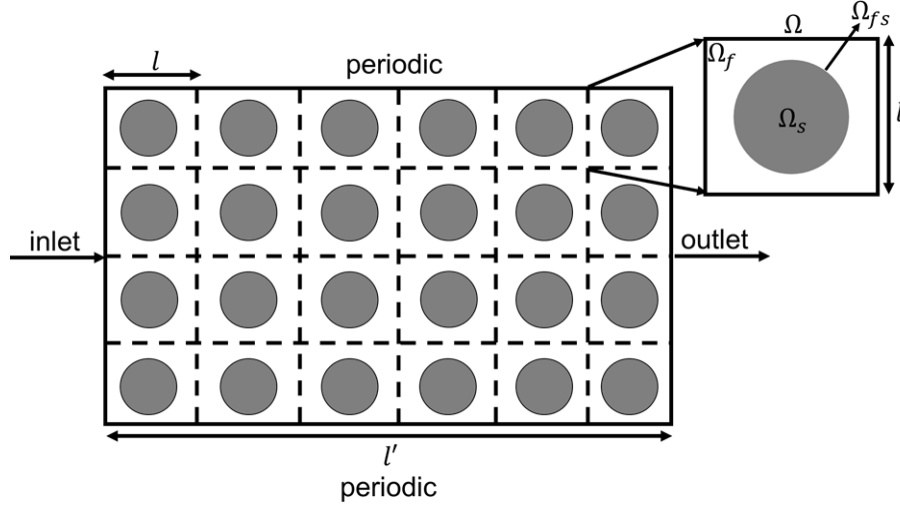
Figure 1. Cross-sectional (2D) representation of macroscale filter with rigid ideal spheres packed in simple-cubic (SC) arrangement to represent filter grains

The SC configuration is suitable to encapsulate the clean bed porosity (θ_0) range of 0.5 – 0.7 for GAC operating filters (MWH, 2005; Voutchkov, 2012; Voutchkov, 2017) as its ultimate contact scenario, whereby each sphere touches one another, results in 0.476 for θ_0. The length of each SC periodic cell (l_{SC}) in Figure 1 is computed as follows.

$$l_{SC} = \sqrt[3]{\frac{\frac{\pi}{6} d_{c,0}^3}{1 - \theta_0}} \quad (2.1)$$

where $d_{c,0}$ is the effective size of each ideal sphere.

Within each SC periodic cell in Figure 1, the fluid motion in the available pore space is governed by the incompressible steady-state Stokes equation at low Reynolds number in (2.2) and mass continuity equation in (2.3).

$$0 = -\frac{1}{\rho}\frac{\partial p^*}{\partial x_i^*} + \frac{\mu}{\rho}\nabla^2 u_i^*, \qquad x \subset \Omega_f(t^*) \quad (2.2)$$

$$\frac{\partial u_i^*}{\partial x_i^*} = 0, \qquad x \subset \Omega_f(t^*) \quad (2.3)$$

where x^* is the position vector, u^* the velocity vector, μ the fluid dynamic viscosity, p^* the fluid pressure, and ρ the fluid density.

The transport of solute (turbidity particles or NOM materials), via advection and diffusion, within $\Omega_f(t^*)$ of each SC periodic cell is described in (2.4). We define the concentration of solute, c^* as mass of solute per unit volume of fluid.

$$\frac{\partial c^*}{\partial t^*} + \frac{\partial(c^* u_i^*)}{\partial x_i^*} = D_p^* \nabla^2 c^*, \qquad x \subset \Omega_f(t^*) \quad (2.4)$$

where D_p^* the unknown particle diffusivity responsible for the depth filter's removal mechanisms (rapid effective filtration, adsorption), and t^* is time.

We introduce a unique boundary condition in (2.5) to account for the concentration of solute undergoing a n order reaction rate on the fluid-solid interface due to the assumed particle diffusion mechanism.

$$-\frac{\frac{\partial S^*}{\partial x_i^*}}{|\nabla S|} \cdot \left(D_p^* \frac{\partial c^*}{\partial x_i^*} \right) = k_{fs}(c^*)^n, \qquad x \subset \Omega_{fs}(t^*) \quad (2.5)$$

where S is the boundary of the sphere, $\frac{\frac{\partial S^*}{\partial x_i^*}}{|\nabla S|}$ the outward normal vector acting on the microscale sphere, k_{fs} the reaction rate occurring on the fluid-solid interface (Ω_{fs}), and n (≥ 0) the order of reaction occurring. It is important to highlight that an increasing n value will violate the linearity of the PDE problem in (2.5), hence we will only analyse the n values of 1 and 2 (assumed to be weakly non-linear) in this study as our first approach.

2.2. Normalization

We then adopt the following scaling variables to normalize (2.2 – 2.5): (i) $c^* = c_{0,tss}c$, (ii) $t^* = Tt$, (iii) $u_i^* = Uu_i$, (iv) $x_i^* = lx_i$, (v) $p^* = Pp$, and (vi) $D_p^* = D_p D$, whereby T, U, P and D_m are the respective scales for the time, velocity, pressure and diffusion parameters, and $c_{0,tss}$ represents the influent's total suspended solids concentration. Three unique macroscopic time scales (T) are also adhered in our analysis: (a) convection time scale (T_c) in (2.6), (b) reaction time scale (T_R) in (2.7), and (c) macroscopic diffusion time scale (T_D) in (2.8).

$$T_c = \frac{l'}{U} \quad (2.6)$$

$$T_R = \frac{l'}{k_{fs}c_{eqm}^{n-1}} \quad (2.7)$$

$$T_D = \frac{(l')^2}{D_p} \quad (2.8)$$

where l' is the characteristic length of the macroscale filter, and k_{fs} adopts the dimensions of $[M^{1-a}L^{3a-2}T^{-1}]$ for generality. The dimensionless microscale Reynolds number (Re), Peclet number (Pe) and Damköhler ($D_{a,l}$) number are also defined in (2.9), (2.10) and (2.11) respectively.

$$Re = \frac{\rho U l}{\mu} \quad (2.9)$$

$$Pe = \frac{Ul}{D_m} \quad (2.10)$$

$$D_{a,l'} = \frac{T_D}{T_R} = \frac{k_{fs} c_{eqm}^{n-1} l}{\varepsilon D_p} = \frac{D_{a,l}}{\varepsilon} \quad (2.11)$$

where $D_{a,l'}$ the macroscale Damköhler number.

Finally, we note that a small length scale (ε) which is defined as $\frac{l}{l'}$ is adopted for the subsequent homogenization procedures. A dominant balance is defined between the macroscale pressure gradient acting upon the depth filter and the viscous flow resistance around the microscale sphere which enables us to derive the homogenized effective Darcy's Law equation subsequently.

3. Homogenization procedures

We adopt the multiple-scale coordinates of x and $x' = \varepsilon x$ whereby x is the fast variable defined within the periodic cell, and x' is the slow variable spanning across the macroscopic domain (Mei and Vernescu, 2012a and 2012b). The perturbation expansions for the fluid parameters (which are all cell-periodic) can be expressed as follows.

$$H = H^{(0)} + \varepsilon H^{(1)} + \varepsilon^2 H^{(2)} + \cdots (3.1)$$

where H can be p, c and u_i.

We then introduce the following spatial derivative to perform the multiple-scale expansions.

$$\frac{\partial}{\partial x_i} \to \frac{\partial}{\partial x_i} + \varepsilon \frac{\partial}{\partial x_i'} \quad (3.2)$$

To demonstrate the homogenization procedure, we succinctly perform the analysis by adopting the time scale of T_c for rapid filtration conditions. The final dimensionless forms of (2.2 – 2.5) are then shown in (3.3a – d) respectively after the appropriate normalization procedures. We note that the extension to slow filtration conditions is achieved by changing the time scale to either T_D or T_R while the homogenization procedures remain unchanged.

$$0 = -\frac{\partial p}{\partial x_i} + \varepsilon \nabla^2 u_i, \qquad x \subset \Omega_f(t) \quad (3.3a)$$

$$\frac{\partial u_i}{\partial x_i} = 0, \qquad x \subset \Omega_f(t) \quad (3.3b)$$

$$\varepsilon \frac{\partial c}{\partial t} + \frac{\partial (c u_i)}{\partial x_i} = Pe^{-1} D \nabla^2 c, \qquad x \subset \Omega_f(t) \quad (3.3c)$$

$$-\frac{\frac{\partial S}{\partial x_i}}{|\nabla S|} \cdot \left(D \frac{\partial c}{\partial x_i} \right) = \varepsilon D_{a,l'} c^n, \qquad x \subset \Omega_{fs}(t) \quad (3.3d)$$

To demonstrate our novelty, we confine our homogenization analysis to the solute transport problem (3.3c – 3.3d) while noting that the analysis for the flow problem (3.3a – 3.3b) can be understood from previous multiscale works (Mei et al., 1996; Mei and Vernescu, 2012a and 2012b; Dalwadi et al., 2015 and 2016) whereby the homogenized dimensionless Darcy's law can be derived systematically.

3.1. Solute problem analysis

By using (3.2), the multi-scale expansion forms (3.3c – 3.3d) are as follows.

$$\varepsilon \frac{\partial}{\partial t} \left(c^{(0)} + \varepsilon c^{(1)} + \cdots \right) + \left(\frac{\partial}{\partial x_i} + \varepsilon \frac{\partial}{\partial x_i'} \right) \left(u_i^{(0)} + \varepsilon u_i^{(1)} + \cdots \right) \left(c^{(0)} + \varepsilon c^{(1)} + \cdots \right)$$
$$= Pe^{-1} D \left(\frac{\partial}{\partial x_j} + \varepsilon \frac{\partial}{\partial x_j'} \right) \left(\frac{\partial}{\partial x_j} + \varepsilon \frac{\partial}{\partial x_j'} \right) \left(c^{(0)} + \varepsilon c^{(1)} + \cdots \right), \quad x$$
$$\subset \Omega_f(t) \quad (3.4a)$$

$$-\frac{\frac{\partial S}{\partial x_i}}{|\nabla S|} \cdot \left(D \left(\frac{\partial}{\partial x_i} + \varepsilon \frac{\partial}{\partial x_i'} \right) \left(c^{(0)} + \varepsilon c^{(1)} + \cdots \right) \right) = \varepsilon D_{a,l'} \left(c^{(0)} + \varepsilon c^{(1)} + \cdots \right)^n,$$
$$x \subset \Omega_{fs}(t) \quad (3.4b)$$

At the leading order of ε^0, $c^{(0)}$ is also determined to be independent of the microscale variations. At the next order of ε^1, we systematically derive the following for (3.4a) and (3.4b) respectively.

$$\theta \frac{\partial c^{(0)}}{\partial t} + \tilde{u}_i^{(0)} \frac{\partial c^{(0)}}{\partial x_i'} = -Pe^{-1} D_{a,l'} C_R c^{(0)^n}, \qquad x \subset \Omega_f(t) \quad (3.5)$$

subject to the boundary condition of (3.6).

$$-\frac{\frac{\partial S}{\partial x_i}}{|\nabla S|} \cdot \left(D\frac{\partial c^{(1)}}{\partial x_i} + D\frac{\partial c^{(0)}}{\partial x_i'} \right) = D_{a,l'} c^{(0)^n}, \qquad x \subset \Omega_{fs}(t) \quad (3.6)$$

where C_R is a proposed dimensionless effective reaction rate which depends on the pore-geometry $\frac{|\Omega_s|}{|\Omega_f|}$ within the periodic cell whereby $|\Omega_s| = \frac{2}{3}\pi d_{c,0}^3$ which represents the volume of the spheres inside the SC periodic cell, and $|\Omega_f|$ represents the volume of fluid within the SC periodic cell.

We then consider the solution for the cell problem of $c^{(1)}$ in the following form (Auriault and Adler, 1995, Equation 40).

$$c^{(1)} = \chi_i \frac{\partial c^{(0)}}{\partial x_i'} + \hat{c}^{(1)} \quad (3.7)$$

where χ_i is the microscale periodic vector field of spatial dimensions, and $\hat{c}^{(1)}$ is an integration constant which is independent of the microscale variations. The microscale variation of $c^{(1)}$ from (3.8) is then expressed as follows.

$$\frac{\partial c^{(1)}}{\partial x_i} = \frac{\partial \chi_k}{\partial x_k}\frac{\partial c^{(0)}}{\partial x_i'} + \chi_i \nabla \cdot \nabla' c^{(0)} \quad (3.8)$$

Substituting (3.8) back into (3.6) results in the following modified form.

$$-\frac{\frac{\partial S}{\partial x_i}}{|\nabla S|} \cdot \left(D\left(\frac{\partial \chi_k}{\partial x_k}\frac{\partial c^{(0)}}{\partial x_i'} + \chi_i \nabla \cdot \nabla' c^{(0)} \right) + D\frac{\partial c^{(0)}}{\partial x_i'} \right) = D_{a,l'} c^{(0)^n}, \qquad x \subset \Omega_{fs}(t) \quad (3.9)$$

At the next order of ε^2, we obtain the following.

$$\theta \frac{\partial c^{(1)}}{\partial t} + \tilde{u}_i^{(0)} \frac{\partial c^{(1)}}{\partial x_i'} + \tilde{u}_i^{(1)} \frac{\partial c^{(0)}}{\partial x_i'}$$
$$= Pe^{-1}\frac{\partial}{\partial x_i'}\left(D\left(\frac{\partial \chi_k}{\partial x_k}\frac{\partial c^{(0)}}{\partial x_i'} + \chi_i \nabla \cdot \nabla' c^{(0)}\right) + D\frac{\partial c^{(0)}}{\partial x_i'}\right)$$
$$- nPe^{-1}D_{a,l'} C_R c^{(0)^{n-1}} c^{(1)}, \qquad x \subset \Omega_f \quad (3.10)$$

subject to the following boundary condition.

$$-\frac{\frac{\partial S}{\partial x_i}}{|\nabla S|} \cdot \left(D\frac{\partial c^{(2)}}{\partial x_i} + D\frac{\partial c^{(1)}}{\partial x_i'} \right) = nD_{a,l'} c^{(0)^{n-1}} c^{(1)}, \qquad x \subset \Omega_{fs}(t) \quad (3.11)$$

We consider the perturbation expansion of the temporal derivative of $\tilde{c}$ within the SC microscale cell as follows.

$$\frac{\partial \tilde{c}}{\partial t} = \frac{\partial \tilde{c}^{(0)}}{\partial t} + \varepsilon \frac{\partial \tilde{c}^{(1)}}{\partial t} + O(\varepsilon^2) \quad (3.12)$$

To further modify (3.12), we adhere to the respective representations of (3.5) and (3.10) to derive the following.

$$\frac{\partial \tilde{c}}{\partial t} = -\tilde{u}_i^{(0)} \frac{\partial c^{(0)}}{\partial x_i'} - \varepsilon \tilde{u}_i^{(1)} \frac{\partial c^{(0)}}{\partial x_i'} - \varepsilon \tilde{u}_i^{(0)} \frac{\partial c^{(1)}}{\partial x_i'} - Pe^{-1} D_{a,l'} C_R c^{(0)^n}$$
$$+ \varepsilon Pe^{-1} \frac{\partial}{\partial x_i'} \left(D \left(\frac{\partial \chi_k}{\partial x_k} \frac{\partial c^{(0)}}{\partial x_i'} + \chi_i \nabla \cdot \nabla' c^{(0)} \right) + D \frac{\partial c^{(0)}}{\partial x_i'} \right)$$
$$- \varepsilon n Pe^{-1} D_{a,l'} C_R c^{(0)^{n-1}} c^{(1)} + O(\varepsilon^2) \ , \qquad x \subset \Omega_f \quad (3.13)$$

By assuming $\nabla' c^{(0)} \approx \nabla' c$ and the following relationships of (3.14) and (3.15), we obtain (3.16) from (3.13).

$$\tilde{u}_i \frac{\partial c}{\partial x_i'} = \tilde{u}_i^{(0)} \frac{\partial c^{(0)}}{\partial x_i'} + \varepsilon \tilde{u}_i^{(0)} \frac{\partial c^{(1)}}{\partial x_i'} + \varepsilon \tilde{u}_i^{(1)} \frac{\partial c^{(0)}}{\partial x_i'} + O(\varepsilon^2) \quad (3.14)$$

$$c^n = c^{(0)^n} + \varepsilon n c^{(0)^{n-1}} c^{(1)} + O(\varepsilon^2) \quad (3.15)$$

$$\frac{\partial \tilde{c}}{\partial t} = -\tilde{u}_i \frac{\partial c}{\partial x_i'} - Pe^{-1} D_{a,l'} C_R c^n + \varepsilon Pe^{-1} \frac{\partial}{\partial x_i'} \left(D \left(\frac{\partial \chi_k}{\partial x_k} \frac{\partial c}{\partial x_i'} + \chi_i \nabla \cdot \nabla' c \right) + D \frac{\partial c}{\partial x_i'} \right)$$
$$+ O(\varepsilon^2) \ , \qquad x \subset \Omega_f \quad (3.16)$$

(3.16) represents the macroscopic effective advection-dispersion-reaction equation which is accurate up to $O(\varepsilon^2)$. We again note that our analysis is confined to the n values of 1 or 2 as our first approach which will be discussed further in the subsequent sections.

4 Experimental design

We perform a series of rapid filtration experiments for model validations. Figure 2 illustrates the simplified version of our filter setups and the general operational mode to remove both turbidity particles and NOMs materials from the intake seawater source. At regular intervals, samples are collected from both filters to measure turbidity, total suspended solids (TSS) and dissolved organic carbon (DOC) concentrations. Likewise, the pressure gradient measurements of between p_1 and p_2, and between p_3 and p_4 are also taken at designated intervals. The biological slow filtration experiments are currently underway, while we have completed a set of rapid filtration experiments for model validations. Readers are referred to Table 1 for the summary of adopted conditions for the rapid filtration experiments conducted by far.
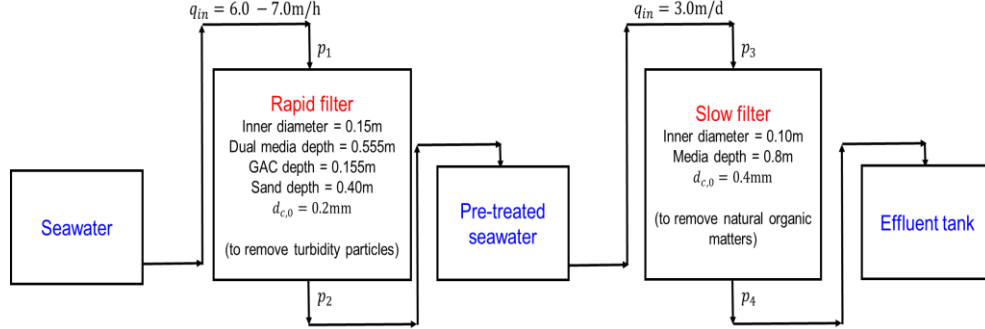
Figure 2. Schematic representation of hybrid rapid and slow granular filters to remove both turbidity particles and natural organic matters from intake seawater

Table 1. Summary of experimental conditions adopted for pre-treatment rapid filtration

Exp no.	q_{in} (m/h)	$c_{0,tur}$ (NTU)	$c_{0,tss}$ (mg/L)	d_p (μm)	Duration $(mins)$
1	8.00	6.63	16.6	83.3	90
2	7.40	2.95	7.38	26.0	90
3	8.15	2.72	6.80	507	90

5   Model Validations

We first modify (3.16) into (5.1) by adopting the following assumptions: (i) quasi-steady-state condition for the discharge concentration from the 0.155m GAC media depth deployed (see Figure 3), (ii) unidirectional flow within the depth filter, (iii) homogeneous clogging inside the filter, (iv) spatial averaging theorem coupled with periodicity boundary conditions, (v) $n = 1$ for rapid effective filtration, (vi) $Pe^{-1} \sim O(\varepsilon)$ which ensures a dominant balance between advection and the regarded particle diffusion at the macroscale, and (vii) $D_{a,l'} \sim O(\varepsilon^{-1})$.

$$0 = -\tilde{u}_3 \frac{\partial c}{\partial x_3'} - C_R c + \varepsilon^2 \frac{\partial}{\partial x_i'}\left(D \frac{\partial c}{\partial x_i'}\right) + O(\varepsilon^2) , \qquad x \subset \Omega_f \quad (5.1)$$

By comparing the respective terms of $O(1)$ of (5.1), we obtain the final solution of (5.2) while including an unknown calibration factor in C_1 to account for the random packing of media grains in the actual depth filter.

$$\tilde{u}_3 = C_1 \frac{C_R x_3'}{\ln(\frac{c_{0,tss}}{c})}, \qquad x \subset \Omega_f \quad (5.2)$$

We then adhere to the dimensionless homogenized Darcy's Law equation in the following with respect to the derived form of (5.2).

$$C_1 \frac{C_R x_3'}{\ln(\frac{c_{0,tss}}{c})} = -K \frac{\partial p^{(0)}}{\partial x_3'}, \qquad x \subset \Omega_f \quad (5.3)$$

Finally, we compute the normalized values (β) of the macroscale dimensionless pressure gradient acting upon the lab-scale depth filter in (5.4) which predicted values generally agree with the respective experimentally-derived values in Figure 4.

$$\beta = \frac{\left(\frac{\partial p^{(0)}}{\partial x_3'}\right)_t}{\left(\frac{\partial p^{(0)}}{\partial x_3'}\right)_0}, \qquad x \subset \Omega_f \quad (5.4)$$
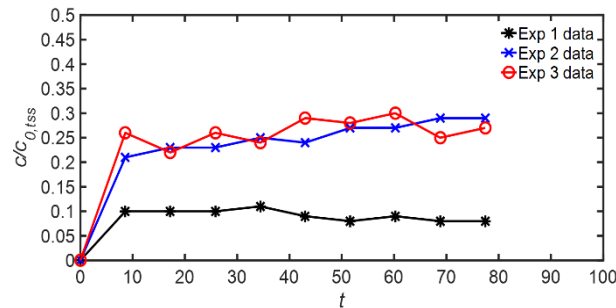
Figure 3. Transient variations of $\frac{c}{c_0}$ at 0.155m GAC media depth
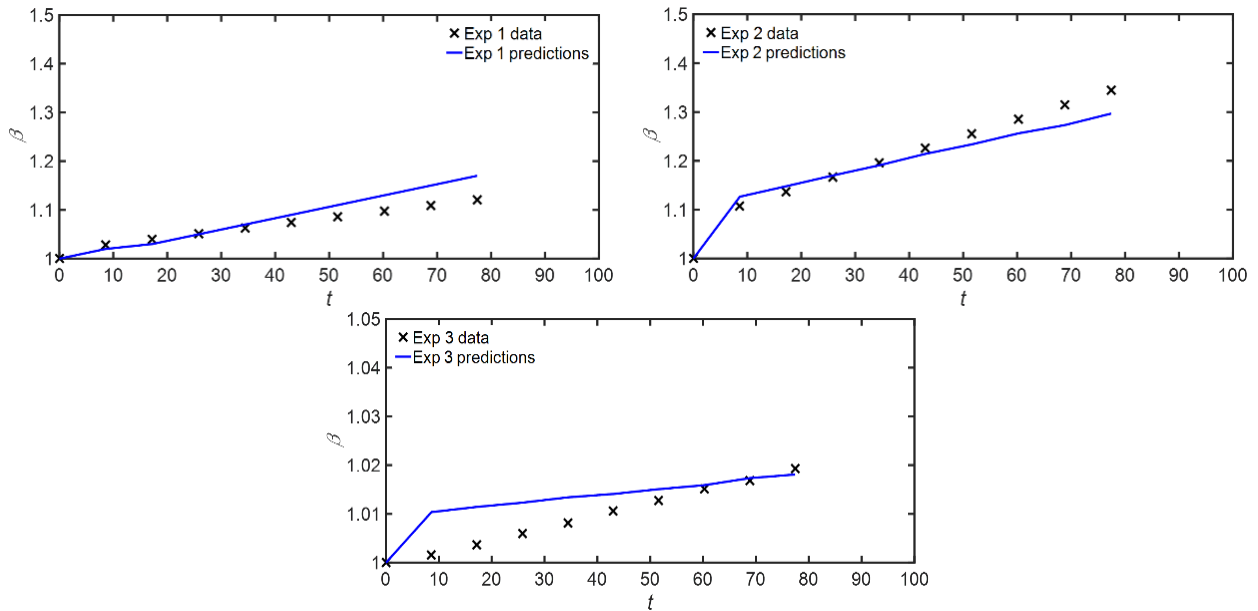
Figure 4. Comparison between predicted and experimental values of β for Exp 1 to 3

With respect to Figure 4, we believe that the agreement will further improve with a higher GAC media depth due to a smaller resultant value in ε.

6   Computational methodology

In this section, we succinctly describe on our computational methodology to resolve for the non-linear microscale problem of c^n for n greater than 2. Computationally, it is not possible to resolve for a numerical domain having fully periodic flow conditions which is required for the periodic cell problem in Figure 1. Hence, we propose to adopt the configurations in Figures 5a to 5c by defining the inlet and outlet zones to the numerical domain as shown. Errors are expected to be incurred due to the imposed boundaries and these errors can gradually be reduced as the length of the domain increases (Figures 5b and 5c) to approach the true ε value. However, emulating the full unidirectional depth of the macroscale filter under periodic flow conditions is computationally expensive. Hence, we hypothesize that there exists a ε' value, but is more than the true ε value, which ensures that the error function is sufficiently small for subsequent predictions.

We perform the simulation runs in OpenFOAM AWS (The OpenFOAM Foundation) which enables us to harness on a large number of computer processes if necessary. Our general methodology is as follows.

  i.   Introducing the homogenized effective solute transport equations (related to c^n) into the incompressible fluid flow solver (*icoFoam*) for coupling the fluid-solute problems
  ii. Introducing a unique boundary condition to account for the solute interactions occurring on the microscale spheres' boundaries
  iii. Develop the basic cell geometry of either SC or FCC of varying lengths using CAD program and the *snappyHexMesh* utility in OpenFOAM
  iv. Perform the simulation runs while varying the number of computational grids for each analysed domain to check on grid convergence
  v.   Total simulation runtime for each analysed domain depends on the velocity scale and ε'
  vi. Time step of simulation run is varied to check on temporal convergence
  vii. Predicted spatial gradient of c^n will be introduced back into the homogenized effective equation to perform the subsequent predictions for the normalized pressure gradient and be compared with the respective experimental values

7   Conclusion

In this study, the multiscale perturbation analysis is coupled with the homogenization theory to model the clogging behaviour of pre-treatment filters in desalination facilities. We have validated our linear homogenization analysis for pre-treatment rapid filtration by comparing the predicted values from the derived effective homogenized equation

with our experimentally-derived values for the normalized pressure gradient acting upon the lab-scale filter under varying conditions. To extend the analysis to non-linear perturbation analysis, a computational methodology is required to resolve the microscale concentration parameter at higher orders which is difficult to do so analytically. This extension component is currently underway. Finally, extension of the model to slow filtration process can be achieved by changing the time scale to either that of reaction time or diffusion time, while retaining the same homogenization procedures to derive the effective homogenized equations for analysis.
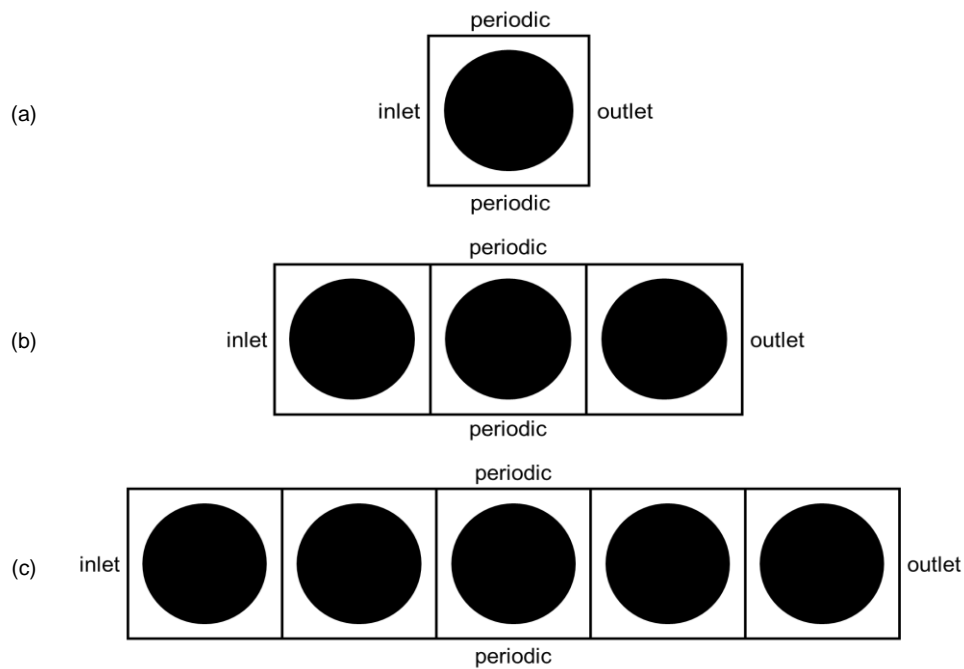
Figure 5. Simplified representation of numerical domains in OpenFOAM to resolve the non-linear microscale problem of c^n: (a) $\varepsilon' \approx 1.00$, (b) $\varepsilon' \approx 0.333$, (b) $\varepsilon' \approx 0.200$.

Acknowledgements

References

1. Auriault, J. L., & Adler, P. M. (1995), "Taylor dispersion in porous media: Analysis by multiple scale expansions," *Advances in Water Resources,* vol. 18(4), pp. 217-226.
2. Dalwadi, M.P., Griffiths, I.M., and Bruna, M. (2015), "Understanding how porosity gradients can make a better filter using homogenization theory," *Proceedings of the Royal Society A: Mathematical, Physical and Engineering Science,* vol. 471 (2182).
3. Dalwadi, M., Bruna, M., and Griffiths, I. (2016), "A multiscale method to calculate filter blockage," *Journal of Fluid Mechanics,* vol. 809, pp. 264-289.
4. Mei, C.C. (1992), "Method of homogenization applied to dispersion in porous media," Transport in Porous Media, vol. 9(3), pp. 261-274.
5. Mei, C.C., Auriault, J. L., and Ng, C.O. (1996), "Some Applications of the Homogenization Theory," In J. W. Hutchinson and T. Y. Wu (Eds.), Advances in Applied Mechanics, Elsevier, vol. 32, pp. 277-348.
6. Mei, C.C., and Vernescu, B. (2012a), "Seepage in Rigid Porous Media," *Homogenization Methods for Multiscale Mechanics*, pp. 85-134.
7. Mei, C.C., and Vernescu, B. (2012b), "Dispersion in Periodic Media or Flows," *Homogenization Methods for Multiscale Mechanics*, pp. 135-178
8. MWH *Water Treatment: Principles and Design*, John Wiley and Sons, Hoboken, New Jersey, 2005, Chapter. 11, pp. 727-818.
9. Ray, N., van Noorden, T., Frank, F., and Knabner, P. (2012), "Multiscale Modeling of Colloid and Fluid Dynamics in Porous Media Including an Evolving Microstructure," Transport in Porous Media, vol. 95(3), pp. 669-696.
10. Royer, P., Auriault, J.-L., Lewandowska, J., and Serres, C. (2002), "Continuum Modelling of Contaminant Transport in Fractured Porous Media," Transport in Porous Media, vol. 49(3), pp. 333-359.
11. *The OpenFOAM Foundation*, http://www.OpenFOAM.org/
12. Voutchkov, N. (2017), "Chapter 8 - Granular Media Filtration," *Pretreatment for Reverse Osmosis Desalination*, pp. 153-186, Amsterdam: Elsevier.